nature structural & molecular biology

Yersinia effector YopO uses actin as bait to phosphorylate proteins that regulate actin polymerization

Wei Lin Lee[1,2], Jonathan M Grimes[2,3] & Robert C Robinson[1,4]

Pathogenic *Yersinia* species evade host immune systems through the injection of *Yersinia* outer proteins (Yops) into phagocytic cells. One Yop, YopO, also known as YpkA, induces actin-filament disruption, impairing phagocytosis. Here we describe the X-ray structure of *Yersinia enterocolitica* YopO in complex with actin, which reveals that YopO binds to an actin monomer in a manner that blocks polymerization yet allows the bound actin to interact with host actin-regulating proteins. SILAC-MS and biochemical analyses confirm that actin-polymerization regulators such as VASP, EVL, WASP, gelsolin and the formin diaphanous 1 are directly sequestered and phosphorylated by YopO through formation of ternary complexes with actin. This leads to a model in which YopO at the membrane sequesters actin from polymerization while using the bound actin as bait to recruit, phosphorylate and misregulate host actin-regulating proteins to disrupt phagocytosis.

Phagocytosis is an essential innate immunity process for the recognition, engulfment and clearance of foreign particles that is driven by actin polymerization[1]. Phagocytosis is activated by the engagement of ligands with phagocytic receptors, through the ligation of IgG-opsonized particles with the Fc receptor (FcγR) or C3bi-opsonized particles with the complement receptor 3 (CR3)[2]. These interactions give rise to the recruitment and/or activation of components that orchestrate actin polymerization beneath the phagocyte membrane to reshape the membrane in order to cover the particle[1]. The actin cytoskeleton contributes force and scaffolding for the formation and closure of the phagocytic cup. The process is orchestrated by a variety of actin-regulating proteins that are recruited to the phagocytic cup at different phases of the membrane-remodeling process. Disruption of protein expression or function leading to impairment of phagocytosis in macrophages has been used to demonstrate the importance of many actin-regulating proteins in this process, including CapG[3], gelsolin[4], diaphanous[5], WASP[6], WIP[7] and VASP[8].

Because actin polymerization is vital to phagocytosis, interfering with actin dynamics is a frequent strategy for pathogen survival within host species. Thwarting macrophage phagocytosis prevents the clearance of bacteria during infection, thus leading to their propagation within the host. Pathogenic *Yersinia* species use type III secretion systems (T3SSs) to inject effector proteins into the cytosol of phagocytic cells, thus interfering with a variety of immune-cell functions to evade host immune systems[9]. One of these pathogenic *Yersinia* species, *Yersinia pestis,* is the causative agent of the bubonic plague, which is estimated to have claimed more than a hundred million lives in numerous pandemics through the course of civilization, including the Plague of Justinian (541–542)[10], the Black Death (1347–1351)[11] and the Third Pandemic (1855–1959)[12]. *Y. pestis* is highly infectious and lethal if left untreated, and in the 21st century it continues to claim lives[13]. Although infections can now be successfully treated with antibiotics, the discovery of strains that have acquired self-transmissible plasmids conferring antibiotic resistance has fueled concerns of the reemergence of *Y. pestis* epidemics[14].

YopO, also known as YpkA, one of the effectors injected by the T3SS, contributes to the disabling of phagocytosis by disruption of the actin cytoskeleton. The phosphorylation activity of YopO is specifically required for the inhibition of *Yersinia* YadA-dependent phagocytosis[15]. YopO has three functional regions: an N-terminal region that targets it to the inner surface of the host-cell plasma membrane (residues 1–88)[16,17]; a region homologous to eukaryotic serine/threonine kinases (residues 115–431)[18,19]; and a Rho GTPase–binding domain (residues 434–729) that serves as a guanine-nucleotide dissociation inhibitor (GDI)[20]. YopO sequesters RhoA and Rac, turning off their activation of the actin-polymerization machineries (although it does not sequester Cdc42)[21]. The structure of YopO's GDI domain was previously elucidated in isolation and in complex with Rac1. In both structures, the GDI region is an elongated helical domain composed of two distinct subdomains held together by a 65-Å-long 'backbone' helix[20]. Both the kinase and the GDI domains interact with actin, and binding to host actin is essential to YopO's kinase activity[15,19]. Cytoplasmic actin stimulates autophosphorylation of YopO more effectively than muscle actin isoforms[15]. Overexpression of YopO in HeLa cells induced actin-filament disruption and cell retraction from the substratum[17,19,21], whereas overexpression of the kinase-dead mutant resulted in an intermediate phenotype[19,20], thus suggesting that YopO affects the actin cytoskeleton through both kinase-dependent and kinase-independent mechanisms[22]. YopO has been found to inhibit $G\alpha_q$ signaling pathways through its kinase activity[23].

[1]Institute of Molecular and Cell Biology, Agency for Science, Technology and Research (A*STAR), Singapore. [2]Division of Structural Biology, Wellcome Trust Centre for Human Genetics, University of Oxford, Oxford, UK. [3]Diamond Light Source, Oxfordshire, UK. [4]Department of Biochemistry, National University of Singapore, Singapore. Correspondence should be addressed to J.M.G. (jonathan@strubi.ox.ac.uk).

Received 10 November 2014; accepted 30 December 2014; published online 9 February 2015; doi:10.1038/nsmb.2964

At present, little is known about the kinase function of YopO or of its kinase substrates.

Here we set out to identify the molecular mechanisms of the kinase domain of YopO. We report the crystal structure of YopO encompassing the kinase and GDI domains in complex with its activator, actin. The structure, together with biochemical data, reveals the GDI-independent mechanisms of YopO. YopO binds to the pointed face of an actin monomer, sterically blocking actin polymerization while using the bound actin as bait to recruit regulators of actin polymerization, thus leading to their phosphorylation and potential misregulation. We then demonstrated that YopO-induced phosphorylation of VASP impairs its ability to accelerate the polymerization of profilin–actin *in vitro*.

RESULTS

Structure determination of the YopO–actin complex

We determined the crystal structure of *Yersinia enterocolitica* YopO encompassing the kinase and GDI domains, bound to actin. *Y. enterocolitica* causes the zoonotic disease yersiniosis, which affects humans, and its YopO shares 97% sequence identity with that from *Y. pestis* (**Supplementary Fig. 1**). Initial crystallization efforts failed to produce crystals suitable for high-resolution structural studies. Surface entropy reduction[24] yielded crystals that diffracted X-rays to 2.65 Å, thus leading to our determination of the structure (**Table 1** and **Supplementary Fig. 2**). The structure revealed that YopO interacts with actin at an unusual site, sandwiching actin subdomain 4 between the GDI and the kinase domains of YopO (**Fig. 1a**). The catalytic cleft of the kinase domain, being flanked between the kinase domain and the GDI domain, which lie ~33 Å apart, potentially restricts the dimensions of the phosphorylation targets that can be inserted into this groove. The YopO–actin complex has an extensive interaction interface of 2,034 Å^2, with the kinase domain (1,220 Å^2) occluding a larger surface area on actin than the GDI domain (814 Å^2). In the YopO–actin complex, actin adopts a native actin–ATP monomer conformation with a typically disordered DNase I–binding loop (residues 40–50)[25]. The interaction of YopO with actin leaves the profilin-binding site on actin unobscured, thus confirming previous studies reporting copurification of profilin with YopO and actin[19].

Table 1 Data collection and refinement statistics

	YopO–actin
Data collection	
Space group	$P2_1$
Cell dimensions	
a, b, c (Å)	70.8, 122.0, 89.3
α, β, γ (°)	90.0, 94.9, 90.0
Resolution (Å)[a]	20.0–2.65 (2.70–2.65)
R_{merge}	0.10 (0.46)
I / σI	12.8 (2.7)
Completeness (%)	95.9 (75.1)
Redundancy	3.6 (3.2)
Refinement	
Resolution (Å)	20.0–2.65
No. reflections	41,791 (3,135)
R_{work} / R_{free}	18.6 / 22.0
No. atoms	
Protein	7,315
Ligand/ion	32
Water	171
B factors (Å^2)	
Protein	48.8
Ligand/ion	37.5
Water	43.5
r.m.s. deviations	
Bond lengths (Å)	0.002
Bond angles (°)	0.60

[a]The data set was collected from one single crystal. Data in parentheses are for the highest-resolution shell.

Conformational changes to the GDI domain upon actin binding

The actin-bound GDI domain maintains its structure as an elongated helical-rich domain, composed of two distinct subdomains held together by the backbone helix, except that the backbone helix (α14) bends by 30°, to result in the translocation of the GDI N-terminal subdomain (helices α14–18) by 30 Å toward actin (as measured for Thr655 on α16 helix) (**Fig. 1b**)[17,20]. In all three GDI structures (actin bound, Rac1 bound and unbound), the conformation of the Rac1-binding interface of YopO appears to be equally accessible (**Supplementary Fig. 2b**), and residues 513–532, which connect helices α11 and α12 are disordered (**Supplementary Fig. 1**). The binding sites on YopO for Rac1 and actin are well separated from each other and from the active site of the kinase domain. This, together with the conservation of the conformation of the Rac1-binding interface, suggests that simultaneous interactions at these three sites may occur (**Fig. 1b**). The interaction of the GDI domain with actin is mediated by the loop between helix α15 and α16 and three (α16–18) of the four helices within the GDI C-terminal subdomain. This is consistent with data indicating that the C-terminal 20 residues of YopO are important for binding to actin (refs. 15,19 and **Fig. 1**).

Interaction of the kinase domain of YopO with actin

The kinase domain adopts the canonical bilobed kinase fold with an N lobe (residues 108–214) and a larger C lobe (residues 215–425) (**Fig. 1d**). The kinase domain is in an active conformation, with a well-defined activation segment (residues 286–308). The first 19 residues (89–107) are disordered and encompass the phosphorylation sites Ser90 and Ser95 (ref. 15; sequence alignment in **Supplementary Fig. 1**). There is no evidence in the electron density map of phosphorylation on the activation segment or elsewhere in the ordered structure. The kinase domain interacts with actin via the back of the C lobe, through the linker between helices α2 and α3 and a long connecting polypeptide chain between helices α4 and α5 (**Fig. 1d** and **Supplementary Note**). The latter appears to be a unique feature among serine/threonine kinases and is an adaptation for interaction with actin (**Supplementary Fig. 2c**). The interaction between actin and the kinase domain appears to contribute to the activation of the kinase domain by the allosteric positioning and stabilization of the activation segment and the catalytic loop, thus providing the structural explanation for actin-induced kinase activation.

Mechanism of actin-monomer sequestration

YopO clamps around actin subdomain 4 (**Fig. 1a**), blocking the pointed face of the actin monomer. Superposition of the structure of YopO bound to an actin monomer onto the structure of the actin filament[26] revealed that the bound monomer is incapable of incorporation into the filament, owing to steric hindrance conferred by YopO, thus precluding the YopO–actin complex from joining the barbed end of a filament (**Fig. 2a**). This provides a structural basis for the inhibition of actin polymerization by YopO that is seen in pyrene-actin assays[15], with nearly complete inhibition at an equimolar ratio of YopO to actin (**Fig. 2b**). YopO nRac, with mutations made to the Rac-interaction interface of YopO (YopO nRac: Y588A N592A E596A)[20], like YopO wild type (WT), abolishes actin

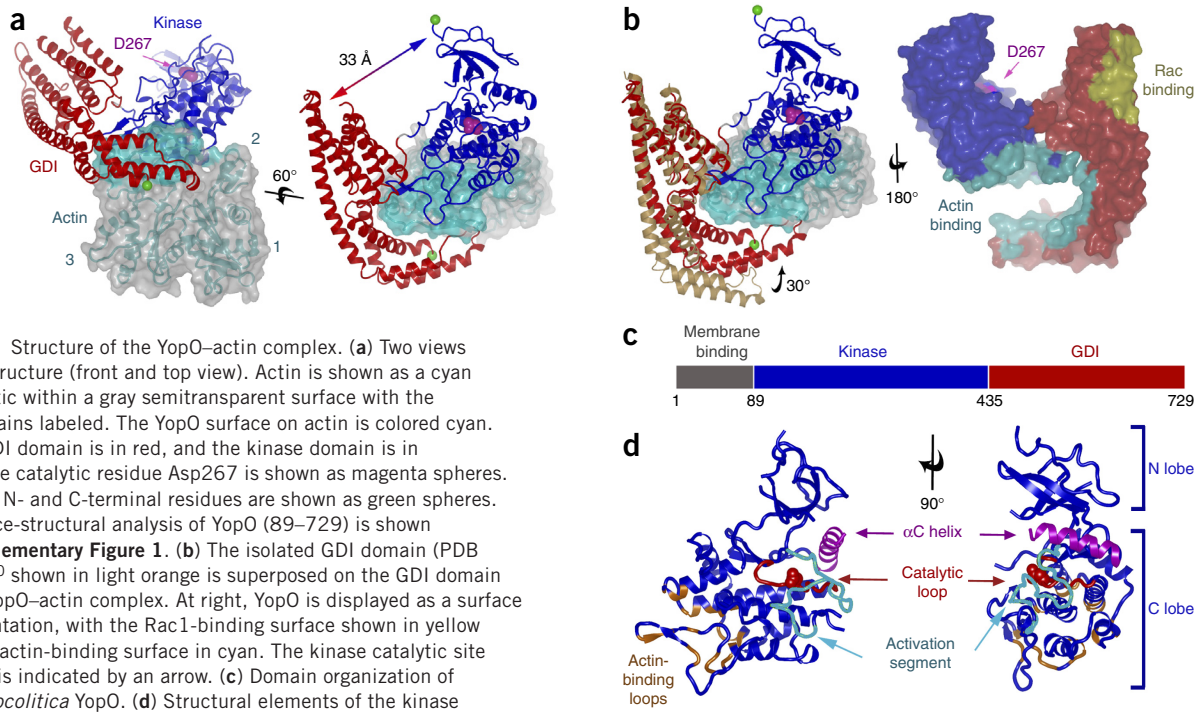

Figure 1 Structure of the YopO–actin complex. (**a**) Two views of the structure (front and top view). Actin is shown as a cyan schematic within a gray semitransparent surface with the subdomains labeled. The YopO surface on actin is colored cyan. YopO GDI domain is in red, and the kinase domain is in blue. The catalytic residue Asp267 is shown as magenta spheres. Ordered N- and C-terminal residues are shown as green spheres. Sequence-structural analysis of YopO (89–729) is shown in **Supplementary Figure 1**. (**b**) The isolated GDI domain (PDB 2H70)[20] shown in light orange is superposed on the GDI domain in the YopO–actin complex. At right, YopO is displayed as a surface representation, with the Rac1-binding surface shown in yellow and the actin-binding surface in cyan. The kinase catalytic site (D267) is indicated by an arrow. (**c**) Domain organization of *Y. enterocolitica* YopO. (**d**) Structural elements of the kinase domain of YopO. The αC helix is shown in purple and the catalytic loop in red, with the catalytic Asp267 shown as spheres and the activation segment shown in cyan. Residues involved, or occluded, in the interaction with actin are shown in orange.

polymerization when at equimolar ratio to actin and is autophosphorylated in the presence of actin (**Fig. 2c**). Mutations introduced to the actin-binding interface of YopO on the basis of the structure (YopO nAct: V374D T376D R723A E727A) greatly reduce YopO's ability to prevent actin polymerization and to autophosphorylate (**Fig. 2b**,**c** and **Supplementary Fig. 3a**), thus confirming the importance of the direct interaction in YopO's sequestration of actin monomers and in G-actin's activation of YopO's kinase activity. Validation that YopO mutants are properly folded is provided by unaltered elution times in gel-filtration chromatography (**Supplementary Fig. 3b**). Unlike Tmod3, which serves as a positive control and inhibits depolymerization through pointed-end capping, YopO does not slow depolymerization and thus does not cap the pointed ends of actin filaments (**Fig. 2d**).

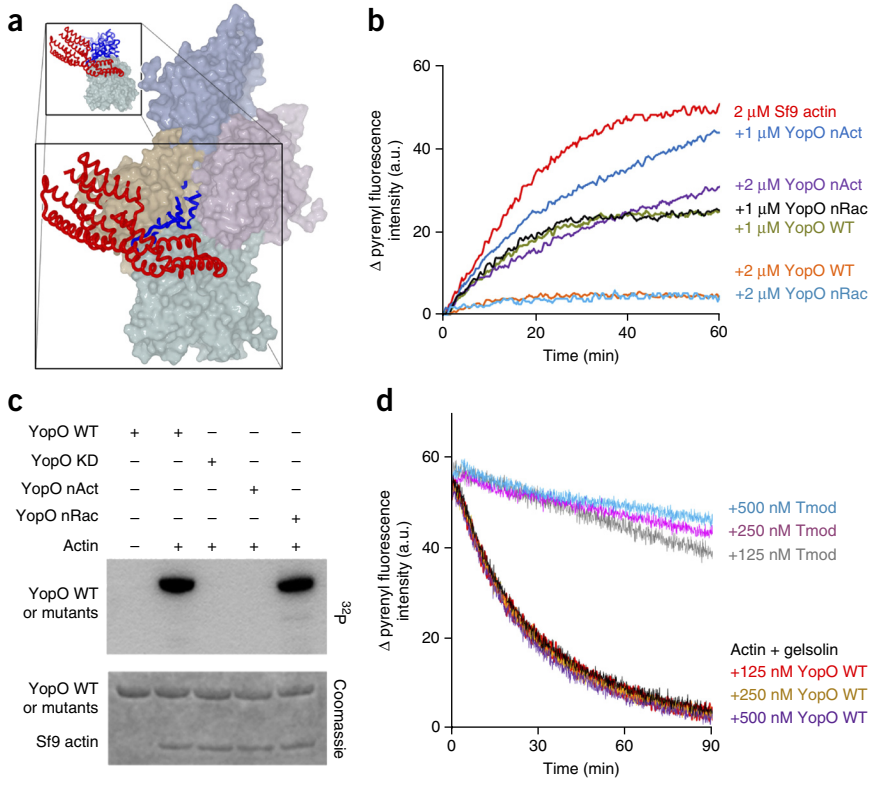

Basis for actin-isoform preference

Rabbit skeletal α-actin is relatively weaker in activating the autophosphorylation of YopO as compared to *Dictyostelium discoideum* or platelet (a mixture of β and γ isoforms) cytoplasmic actins[15]. The YopO–actin structure clarifies the differential activation of YopO by cytoplasmic versus muscle actin isoforms. Sequence alignment of homologous actins—cytoplasmic isoforms (human β-actin, mouse

Figure 2 The YopO–actin complex is polymerization incompetent. (**a**) Superimposition of the YopO–actin complex on the actin filament[26]. YopO is colored as in **Figure 1a**, and the actin filament is represented as a molecular surface. (**b**) Spectrofluorimetry assay using pyrene-labeled actin to monitor the polymerization of Sf9 actin in the presence of YopO WT and mutants. nRac, non-Rac-binding mutant; nAct, reduced-actin-binding mutant; KD, kinase-dead mutant. (**c**) Autophosphorylation of YopO WT and mutants in the presence or absence of actin, monitored by autoradiography and Coomassie staining. (**d**) Pointed-end capping assay of YopO. Tmod, human tropomodulin-3; a.u., arbitrary units; Δ, change.

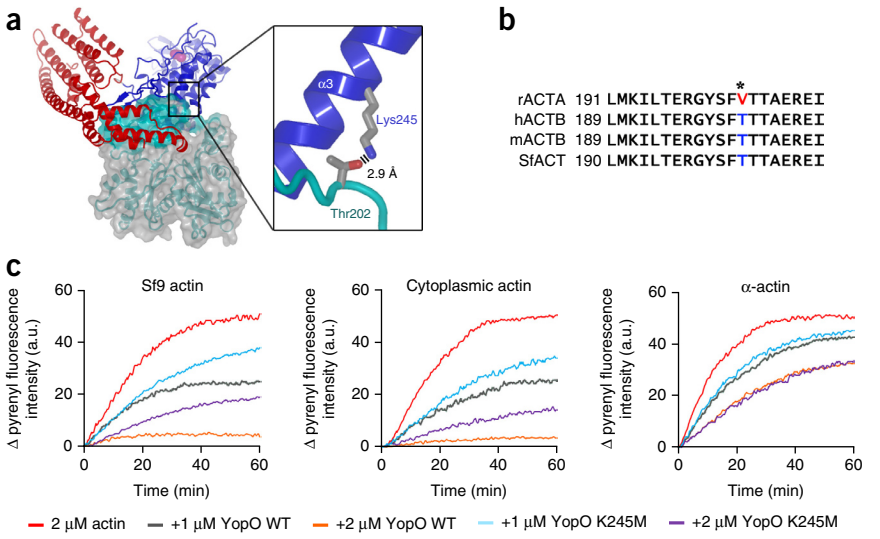

Figure 3 Structural basis of differential actin isoform preference of YopO. (**a**) Thr202 of Sf9 actin forms a hydrogen bond with Lys245 on helix α3 of YopO with a bond length of 2.9 Å. YopO is colored as in **Figure 1a**. (**b**) Sequence alignment of actins. rACTA, rabbit skeletal α-actin; hACTB, human β-actin; mACTB, mouse β-actin; SfACT, *S. frugiperda* actin. Thr202 of Sf9 actin is marked with an asterisk. The entire sequence alignment can be found in **Supplementary Figure 4**. (**c**) Pyrene-actin polymerization assay for the determination of the monomer sequestration activity of different actin isoforms by YopO WT and K245M. Δ, change; a.u., arbitrary units.

β-actin, *Spodoptera frugiperda* (Sf9) actin and *D. discoideum* actin) and a muscle isoform (rabbit skeletal α-actin)—yielded a number of candidate residues that are conserved among cytoplasmic isoforms but are different in the muscle isoform (**Supplementary Fig. 4**). One of these residues is involved in a direct interaction with YopO. Thr202 is conserved in *S. frugiperda* and *D. discoideum* actins and in the corresponding positions in human β-actin (Thr201) and mouse β-actin (Thr201). In the YopO–actin structure, actin Thr202 forms a hydrogen bond with Lys245 of YopO with a bond length of 2.9 Å (**Fig. 3a**). The corresponding residue is Val203 in rabbit α-actin, which is unable to form a side chain hydrogen bond with lysine (**Fig. 3b**).

To test the hypothesis that the ability to form a hydrogen bond between Lys245 of YopO and Thr202 of actin contributes to the differentiation between muscle and nonmuscle actin isoforms, we designed a mutant, YopO K245M, to abolish this hydrogen bond. We tested YopO WT and K245M for the ability to sequester actin in a polymerization assay and found that the sequestration activity of the K245M mutant toward human cytoplasmic actin and Sf9 actin is attenuated in the polymerization assay compared to that of YopO WT (**Fig. 3c**). In contrast, YopO WT and K245M sequester rabbit α-actin to a similar extent. This confirms that the hydrogen bond between Lys245 of YopO and Thr202 of actin confers upon YopO the ability to distinguish between muscle and cytoplasmic actin isoforms and provides a structural basis for the differential autophosphorylation of YopO in the presence of muscle and cytoplasmic actin isoforms[15].

YopO-bound actin interacts with other actin-binding proteins

The majority of actin-regulating proteins bind to actin between subdomains 1 and 3 (refs. 27,28), whereas the binding of YopO to actin leaves this region unobstructed. This prompted an investigation via quantitative proteomics into the interaction of YopO with actin and other actin-binding proteins. We used histidine-tagged YopO to affinity purify endogenous actin and interacting partners from macrophage Raw264.7 cell lysate via stable-isotope labeling of amino acids in cell culture (SILAC) followed by MS analysis[29]. Proteins that were enriched above a cutoff normalized heavy/light (H/L) ratio of 4 include actin and Rac2 as well as many actin-binding proteins including profilin; the filament elongators EVL and VASP; the formins diaphanous 1 (mDia1) and INF2; the Arp2/3-complex activator WASP and the WASP-binding protein WIP; the severing protein gelsolin; and the depolymerizing protein cofilin1 (**Table 2**). Superposition of the structures of actin in complex with profilin and the G-actin–binding domain of VASP (structure from ref. 30) (**Fig. 4a**), gelsolin domains 1–3 (structure from ref. 31) (**Fig. 4b**) and a WH2 motif (structure from ref. 32; further structural description in ref. 33) (**Fig. 4c**), with the YopO–actin complex revealed no steric clashes. This supports the notion that these actin-binding proteins may form ternary complexes with YopO through binding directly to actin. We tested the formation of ternary complexes with YopO–actin for a subset of proteins identified in **Table 2**. A number of them were stable enough to be reproduced on size-exclusion chromatography with purified proteins, including profilin, gelsolin domain 1, cofilin and CapG (**Fig. 4d–g**).

YopO nRac behaves like YopO WT in sequestering G-actin in the pyrene-actin polymerization assay and in autophosphorylation in the *in vitro* phosphorylation assay (**Fig. 2b,c**), thus suggesting that Rac sequestration is independent of actin binding and kinase activation. Affinity purification with histidine-tagged YopO nRac against the

Table 2 YopO recruits actin-binding proteins through actin

		YopO WT			YopO nRac		
		Unique peptides	s.d.[a]	Normalized H/L ratio[b]	Unique peptides	s.d.	Normalized H/L ratio
Rho GTPases	Rac2	4	7.0	33.3	**NF**	**NF**	**NF**
Actin and actin-binding proteins	Actin	136	2.4	25.0	322	2.1	14.3
	Profilin1	20	11.4	25.0	8	1.1	14.3
	EVL	5	15.3	25.0	4	3.3	12.5
	VASP	14	7.2	25.0	14	2.0	12.5
	mDia1	10	0.9	4.5	2	1.4	9.1
	INF2	4	2.6	20.0	**NA**	**NA**	**NA**
	WASP	9	1.2	11.1	8	1.5	11.1
	WIP	2	0.3	5.9	2	0.0	10.0
	Gelsolin	22	6.6	20.0	6	2.7	20.0
	Cofilin1	4	0.8	14.3	3	0.1	10.0
	Twinfilin1	**10**	**0.2**	**2.9**	2	1.5	11.1
	Twinfilin2	**31**	**0.4**	**1.7**	8	0.4	8.3
	CapG	**NF**	**NF**	**NF**	2	0.7	14.3
	CAP1	**35**	**0.1**	**2.3**	21	0.7	6.7
Non-actin-binding proteins	Plcg2	6	0.9	9.1	**NF**	**NF**	**NF**
	Nme1	**18**	**0.1**	**0.5**	2	0	5.0

[a]s.d., with *n* value as the number of unique peptides. [b]Normalized H/L ratio is the inverse weighted-average ratio[44] and represents the relative abundance of the heavy to the light peptides identified for each protein. NF, not found; i.e., peptides corresponding to the protein were not identified in the MS. NA, not available, owing to either the peak at MS1 level being below the noise level or to coelution occurring with other peptides with the same *m/z* and preventing intensity from being measured. Bold type, values below the cutoff of normalized H/L ratio of 4. nRac, non-Rac-binding mutant.

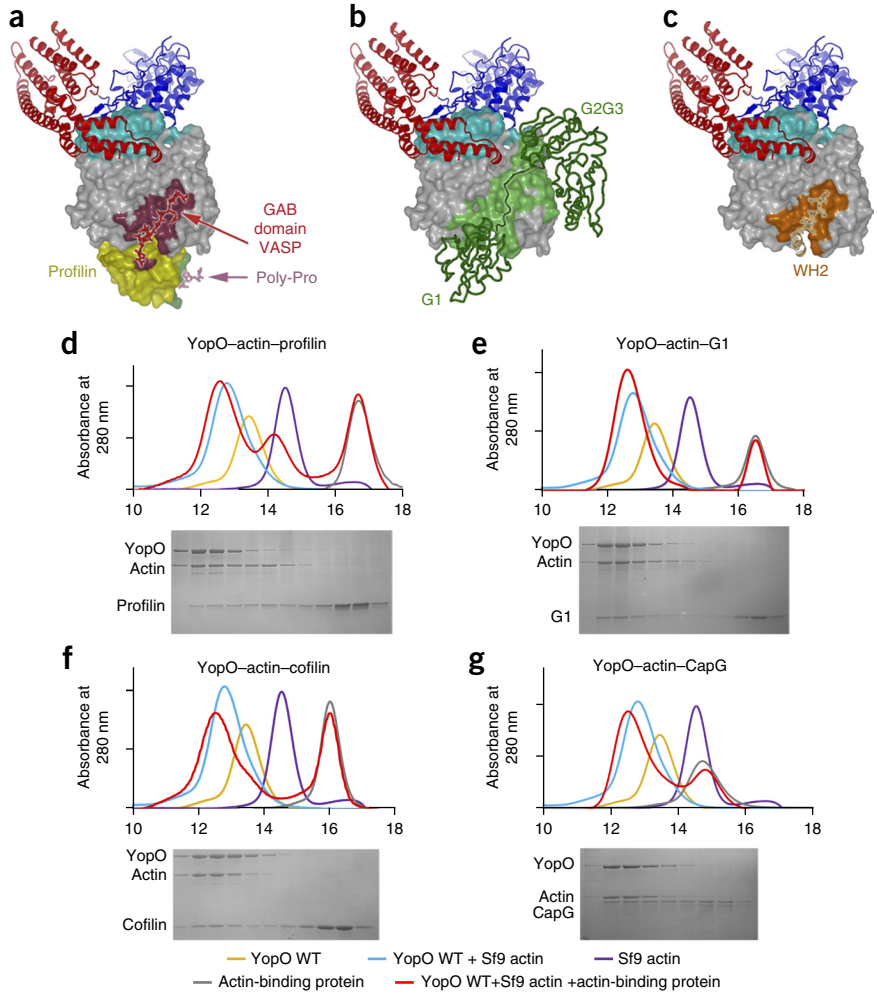

Figure 4 YopO-bound actin interacts with other actin-binding proteins. (**a**) Model of the quaternary complex of YopO–actin–profilin–VASP fragment[30], following the color scheme in **Figure 1a**, with profilin shown in yellow. The surfaces occluded by the actin-binding VASP peptide (red) and profilin-binding polyproline peptide (pink) are colored burgundy and green, respectively. GAB domain, G-actin–binding domain. (**b**) Model of the tricomplex of YopO–actin–gelsolin, with gelsolin in green[31]. G1–3, gelsolin domains 1–3. (**c**) Model of the ternary complex of YopO–actin–WH2, with the WH2 peptide of WASP in ocher[32]. Models of the ternary complexes of YopO–actin–G4–6 and YopO–actin–ADFH can be found in **Supplementary Figure 5a**,**b**. (**d**–**g**) Ternary-complex formation of YopO–actin–profilin (**d**), YopO–actin–G1 (**e**), YopO–actin–cofilin (**f**) and YopO–actin–CapG (**g**), as shown by size-exclusion chromatography. These gel-filtration chromatograms are shown in red and are superimposed on chromatograms of YopO WT, Sf9 actin, YopO WT with Sf9 actin, and the individual actin-binding proteins, colored as indicated. Fractions of the eluted material were analyzed by SDS-PAGE and visualized by Coomassie staining.

Raw264.7 cell lysate yielded a similar profile of actin-binding proteins as YopO WT in the SILAC MS analysis, without enrichment of Rac (**Table 2**). Indeed, all of the common high-confidence interaction partners between the MS data sets in **Table 2** were either actin or actin-binding proteins. As such, actin binding and recruitment of actin-binding proteins by YopO occurs independently of Rac sequestration.

YopO uses actin as bait for phosphorylation

The ability of YopO to be activated by actin and to recruit a multitude of actin-binding proteins, coupled with the positioning of the catalytic cleft of the kinase domain proximal to actin, suggests that YopO may use actin as bait for the recruitment of kinase substrates. We tested a subset of proteins identified to form ternary complexes with YopO–actin (**Table 2**) to identify substrates for phosphorylation by YopO. We incubated purified proteins, or protein fragments, with YopO and insect cytoplasmic Sf9 actin in the presence of [γ-^{32}P]ATP in *in vitro* phosphorylation assays. VASP, EVL, mDia1, WASP and gelsolin were phosphorylated, whereas CapG and Twf1 remained unmodified (**Fig. 5a**). To test the hypothesis that YopO uses actin as bait for the recruitment of substrates, we added a three-fold molar excess of gelsolin domain 1 (G1) to the phosphorylation assay to compete for binding to actin and, in a parallel experiment, added a three-fold molar excess of profilin. G1 binds to actin between subdomains 1 and 3 (K_d = 5 pM)[34] and forms a ternary complex with YopO–actin (**Fig. 4b**,**e**). It acts as a competitor for the common binding site of VASP (**Fig. 4a**), EVL, WASP (**Fig. 4c**), gelsolin and mDia1 on actin, which lies between subdomains 1 and 3 (refs. 27,28). In agreement with the bait hypothesis, the phosphorylation of VASP, EVL, WASP, gelsolin and mDia1 was substantially reduced in the presence of competition from excess G1. The presence of G1 does not disrupt the YopO-actin interaction, because the autophosphorylation of YopO remained robust (**Fig. 5a**). As a comparison, we used profilin in place of G1, because profilin–actin comprises the major part of the polymerization-competent G-actin pool within cells[28]. Profilin also binds actin between subdomains 1 and 3 (K_d = 0.7 μM)[35] in a tricomplex with YopO (**Fig. 4a**,**d**) but is compatible with binding to VASP, EVL, mDia1 and WASP, because these proteins contain polyproline regions that can interact with profilin–actin. VASP, EVL, WASP, gelsolin and mDia1 were able to be phosphorylated in the presence of excess profilin (**Fig. 5a**). Indeed, mDia1 appears to show enhanced phosphorylation in the presence of profilin. Thus, the phosphorylation of substrates by YopO is dependent on their recruitment by actin, and/or profilin–actin, in order to present them to the kinase domain (**Fig. 5b**). Profilin (**Fig. 4a**), Twf1, which consists of two ADF-H domains (**Supplementary Fig. 5**), and CapG, which consists of three gelsolin domains (**Fig. 4g** and **Supplementary Fig. 5**), are not sufficiently elongated to span from the actin-binding site to the kinase catalytic cleft in order to be phosphorylated by YopO–actin.

Phosphorylated VASP is attenuated in actin polymerization

Finally we examined the effect of YopO phosphorylation on VASP-mediated actin polymerization. We used YopO's preference between actin isoforms to differentiate between actin sequestration and phosphorylation by YopO. The use of rabbit skeletal α-actin minimized the effect of polymerization-incompetent YopO–actin, because skeletal actin is sequestered only weakly by YopO (**Fig. 3c**). We pre-incubated YopO with Sf9-cell cytoplasmic actin and VASP in the

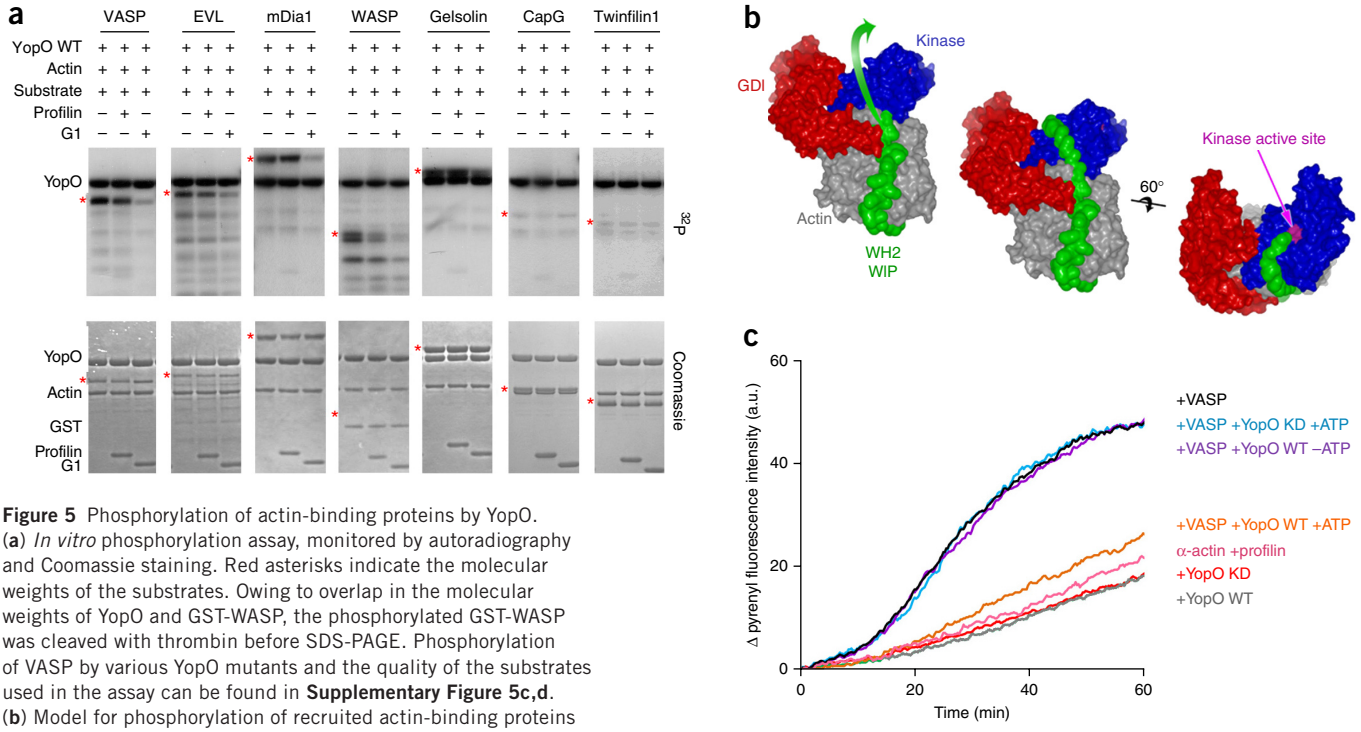

Figure 5 Phosphorylation of actin-binding proteins by YopO. (**a**) *In vitro* phosphorylation assay, monitored by autoradiography and Coomassie staining. Red asterisks indicate the molecular weights of the substrates. Owing to overlap in the molecular weights of YopO and GST-WASP, the phosphorylated GST-WASP was cleaved with thrombin before SDS-PAGE. Phosphorylation of VASP by various YopO mutants and the quality of the substrates used in the assay can be found in **Supplementary Figure 5c,d**. (**b**) Model for phosphorylation of recruited actin-binding proteins by YopO. YopO is colored as in **Figure 1a**, with actin in gray. The WH2 peptide of WIP (PDB 2A41)[32] is drawn in green, at left. Middle and right show an additional modeled 15-residue peptide binding up and into the kinase active site (colored magenta). (**c**) Effect of YopO phosphorylation on VASP-mediated actin polymerization. KD, kinase dead.

presence of Mn–Mg-ATP, to allow the phosphorylation of VASP by YopO, before addition to α-actin and initiation of polymerization. YopO-phosphorylated VASP (0.25 μM) exhibited a substantial reduction in the acceleration of polymerization of α-actin (2 μM) in the presence of excess profilin (2.8 μM), as compared to that obtained with the kinase-dead YopO mutant (YopO KD, D267A K269A) or in the absence of Mn–Mg-ATP in the phosphorylation mix (**Fig. 5c**). Thus, phosphorylation allows YopO to directly target and diminish the activity of this actin-filament elongator in this *in vitro* assay.

DISCUSSION

Here we have presented the X-ray structure of *Y. enterocolitica* YopO in complex with its activator, actin (**Fig. 1** and **Table 1**). The structure reveals that the kinase and GDI domains of YopO sandwich actin subdomain 4, providing the structural basis for actin sequestration and the activation of kinase activity of YopO (**Figs. 1** and **2**). The structure also indicates the basis of the differences in efficiencies of activation of YopO by muscle and cytoplasmic actin isoforms (**Fig. 3**)[15]. The binding of YopO to actin sterically inhibits polymerization of the bound actin yet allows the bound actin to interact with various proteins that regulate actin polymerization, including filament elongators, formins, nucleation-promoting factors, severing proteins and depolymerizing proteins. This suggests that through binding actin these actin-regulating proteins are sequestered by YopO (**Table 2** and **Fig. 4**). In addition, we have determined that a subset of these proteins, including VASP, EVL, WASP, gelsolin and formin mDia1, are recruited and phosphorylated by YopO in a manner that requires the use of the bound actin as bait (**Fig. 5**), which in the case of VASP leads to reduced activity *in vitro*. Although the contribution of YopO to virulence has been debated[18,20,36], these data provide mechanistic insights into the inhibition of phagocytosis by YopO via modulation of actin polymerization. We propose that YopO has the ability to disrupt phagocytosis via (i) inhibiting signal transduction through sequestration of Rac and Rho[21]; (ii) inhibiting polymerization at the site of host-pathogen contact through sequestration of actin; and (iii) phosphorylating actin regulators to misregulate polymerization (**Fig. 6**).

Many pathogens have developed ways to manipulate the actin-polymerization machinery to aid their life cycles. The apicomplexan parasite *Toxoplasma* secretes toxofilin, which regulates host actin filament–assembly dynamics[37], whereas a number of pathogenic bacteria

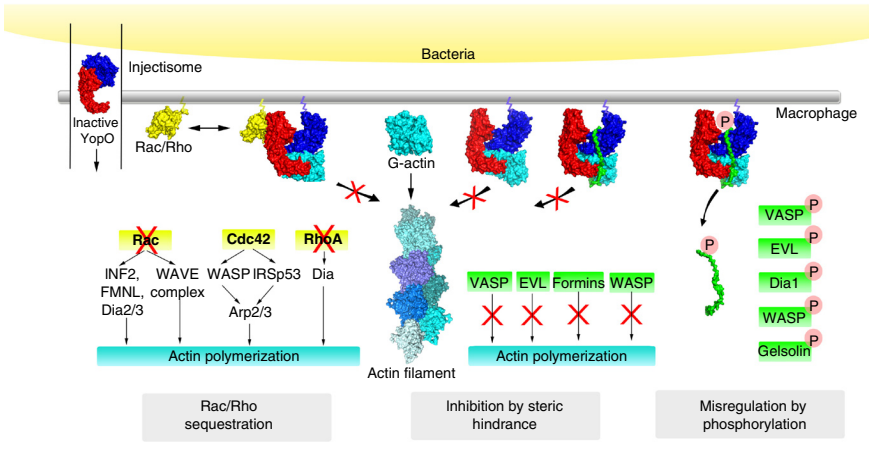

Figure 6 Model for disabling actin polymerization by YopO. P, phosphorylation; Rac/Rho, Rac and/or Rho.

have developed toxins, i.e., actin ADP-ribosylating toxins and actin cross-linking toxins[38], that directly target actin (comparison of their binding interfaces on actin in **Supplementary Fig. 6a**,**b**). YopO takes advantage of the sequence conservation of eukaryotic actin to potentially jump between host species. The stage of disease progression, the transmission and the species within which the actions of YopO are most important have yet to be resolved. The bubonic plague is passed from rats to humans via fleas; this resulted in *Y. pestis* claiming the lives of an estimated 30–60% of the European human population during the 14th century. Because rat and human cytoplasmic actins share 100% identity, the activities of YopO may be relevant across a range of mammalian species.

Many actin-cytoskeletal components have been reported to be regulated by phosphorylation, including WASP and WIP[39], VASP and EVL[40], CapG and gelsolin[41] and mDia1 (ref. 42). This work has shown that YopO phosphorylates WASP, VASP, gelsolin and mDia1, whereas WIP and INF2 have yet to be assayed. This gives rise to the hypothesis that YopO hijacks native phosphorylation pathways that occur under nonpathogenic conditions to exert control over actin-cytoskeletal dynamics. Hence, YopO is likely to prove to be a valuable tool for the study of phosphoregulatory mechanisms of native actin-filament assembly and disassembly machineries.

The location of self-phosphorylation sites outside of the core kinase domain, combined with the paucity of interactions between the kinase and GDI domains in the actin-bound structure, suggests that YopO may acquire an alternative autoinhibited conformation in the absence of actin (**Supplementary Fig. 6c**). We hypothesize that before binding actin, residues 89–107, containing autophosphorylated residues Ser90 and Ser95, fold back onto the catalytic cleft as an autoinhibitory sequence. Given the conformation differences between the reported GDI domain[20] and the GDI domain in the YopO–actin complex, we speculate that binding of actin would induce a multistage activation process, which includes bending of the backbone helix of the GDI domain and further conformational changes that lead to sandwiching of actin between the two domains. The reorganization of domains induced by actin binding would result in the orientation of the catalytic elements within the kinase domain into the active state, and this in turn would lead to autophosphorylation of residues Ser90 and Ser95 and release of the autoinhibition sequence, thus giving rise to the kinase substrate-binding groove being exposed.

The structure of the YopO–actin complex is concordant with previously reported mutation and deletion studies that were used to map out the relative contributions of the GDI and the kinase domains. Constructs comprising solely the GDI domain give rise to an intermediate phenotype of cytoskeletal disruption compared to that of YopO WT[20], whereas constructs with just the kinase domain no longer cause cytoskeletal disruption[43]. These data led to the conclusion that the GDI domain is the dominant contributor to actin-cytoskeletal disruption[20,43]. The YopO–actin structure reveals that this conclusion is only part of the mechanism, because actin sequestration and phosphorylation require a functional actin-binding interface including both the GDI and kinase domains. This structure also clarifies the low level of cytoskeletal disruption that was previously observed with dual mutations to the catalytic residues of the kinase domain and the Rac-binding interface of YopO[20]. This can be attributed to the sequestration of actin by YopO, an activity independent of kinase and GDI functions. This work also supports the observations that overexpression of the YopO kinase-dead mutant gives rise to a reduction, and not total abrogation, of filament disruption[19,20]; this difference is due to the phosphorylation of actin-binding proteins by YopO, which modulates the activities of effector proteins, particularly those not downstream of Rac and RhoA signaling, such as VASP, EVL and gelsolin.

When taken together, these data suggest the series of events that lead to YopO inhibition of phagocytosis. YopO is produced in the bacteria as an inactive agent[17]. Upon injection into the mammalian cell through the T3SS, YopO senses the environment of the host cytoplasm through binding to actin, hence leading to kinase activation, and localizes via the membrane-association domain to the inner surface of the plasma membrane proximal to the bacterium site of attachment[16,43] (model in **Fig. 6**). YopO is further restricted in its localization to areas of actin polymerization through binding to Rac and RhoA[21] while inhibiting Rac- and Rho-mediated actin assembly in the phagocytic cup[43]. YopO's sequestration of G-actin prevents its integration into a filament, yet the YopO–actin complex binds freely to VASP, EVL, formins, WASP and WIP. We hypothesize that binding of these proteins to YopO-sequestered polymerization-incompetent G-actin blocks their activities at the membrane, halting the actin polymerization–driven membrane deformation necessary for phagocytosis. Because the YopO–actin complex is localized at the membrane at the *Yersinia* contact site, through the membrane-targeting domain and interactions with Rho and Rac, a relatively low amount of injected YopO would be effective relative to a freely diffusible effector. In addition, the actin-activated YopO kinase domain phosphorylates these actin polymerization–regulatory proteins, to result in misregulation of cellular actin dynamics upon release from YopO. Thus, YopO counteracts host defenses by launching a three-pronged attack on disrupting actin dynamics within the macrophage: inhibiting signaling, blocking polymerization at the site of host-pathogen contact and misregulating the actin-remodeling machineries via phosphorylation. These combined actions may be expected to contribute to the inhibition of phagocytosis to prevent the clearance of *Yersinia* in the host.

METHODS

Methods and any associated references are available in the online version of the paper.

Accession codes. Coordinates and structure factors have been deposited in the Protein Data Bank under accession code PDB 4CI6.

Note: Any Supplementary Information and Source Data files are available in the online version of the paper.

ACKNOWLEDGMENTS

We thank L. Burtnick and W. Burkholder for discussions and critical reading of the manuscript. W.L.L. and R.C.R. thank the A*STAR for support. We acknowledge the Joint Centre for Structural Biology, Singapore, which is supported by Nanyang Technological University and the Biomedical Research Council (BMRC) of A*STAR, for providing research facilities and P. Kaldis for providing help and facilities for the kinase assays. We thank the Diamond Light Source (proposal MX8423) for crystal screening and beamline BL13B1 at the National Synchrotron Radiation Research Center, Taiwan (NSRRC) for final data collection. The Wellcome Trust Centre for Human Genetics is supported by the Wellcome Trust Core award (090532/Z/09/Z). We thank L. Blanchoin (Institut de Recherches en Technologies et Sciences pour le Vivant) and M. Hernandez-Valladares (University of Liverpool) for reagents.

AUTHOR CONTRIBUTIONS

W.L.L. carried out the experimental work. All authors analyzed the data and prepared the manuscript.

COMPETING FINANCIAL INTERESTS

The authors declare no competing financial interests.

1. Aderem, A. & Underhill, D. Mechanisms of phagocytosis in macrophages. *Annu. Rev. Immunol.* **17**, 593–623 (1999).
2. Griffin, F.M., Griffin, J.A., Leider, J.E. & Silverstein, S.C. Studies on the mechanism of phagocytosis: requirements for circumferential attachment of particle-bound ligands to specific receptors on the macrophage plasma membrane. *J. Exp. Med.* **142**, 1263–1282 (1975).
3. Witke, W., Li, W., Kwiatkowski, D.J. & Southwick, F.S. Comparisons of CapG and gelsolin-null macrophages: demonstration of a unique role for CapG in receptor-mediated ruffling, phagocytosis, and vesicle rocketing. *J. Cell Biol.* **154**, 775–784 (2001).
4. Serrander, L. *et al.* Selective inhibition of IgG-mediated phagocytosis in gelsolin-deficient murine neutrophils. *J. Immunol.* **165**, 2451–2457 (2000).
5. Colucci-Guyon, E. *et al.* A role for mammalian diaphanous-related formins in complement receptor (CR3)-mediated phagocytosis in macrophages. *Curr. Biol.* **15**, 2007–2012 (2005).
6. Lorenzi, R., Brickell, P.M., Katz, D.R., Kinnon, C. & Thrasher, A.J. Wiskott-Aldrich syndrome protein is necessary for efficient IgG-mediated phagocytosis. *Blood* **95**, 2943–2946 (2000).
7. Tsuboi, S. & Meerloo, J. Wiskott-Aldrich syndrome protein is a key regulator of the phagocytic cup formation in macrophages. *J. Biol. Chem.* **282**, 34194–34203 (2007).
8. Coppolino, M.G. *et al.* Evidence for a molecular complex consisting of Fyb/SLAP, SLP-76, Nck, VASP and WASP that links the actin cytoskeleton to Fcγ receptor signalling during phagocytosis. *J. Cell Sci.* **114**, 4307–4318 (2001).
9. Cornelis, G.R. Molecular and cell biology aspects of plague. *Proc. Natl. Acad. Sci. USA* **97**, 8778–8783 (2000).
10. Harbeck, M. *et al. Yersinia pestis* DNA from skeletal remains from the 6th century AD reveals insights into Justinianic Plague. *PLoS Pathog.* **9**, e1003349 (2013).
11. Haensch, S. *et al.* Distinct clones of *Yersinia pestis* caused the black death. *PLoS Pathog.* **6**, e1001134 (2010).
12. Perry, R.D. & Fetherston, J.D. *Yersinia pestis*: etiologic agent of plague. *Clin. Microbiol. Rev.* **10**, 35–66 (1997).
13. Butler, T. Plague gives surprises in the first decade of the 21st century in the United States and worldwide. *Am. J. Trop. Med. Hyg.* **89**, 788–793 (2013).
14. Galimand, M., Carniel, E. & Courvalin, P. Resistance of *Yersinia pestis* to antimicrobial agents. *Antimicrob. Agents Chemother.* **50**, 3233–3236 (2006).
15. Trasak, C. *et al. Yersinia* protein kinase YopO is activated by a novel G-actin binding process. *J. Biol. Chem.* **282**, 2268–2277 (2007).
16. Letzelter, M. *et al.* The discovery of SycO highlights a new function for type III secretion effector chaperones. *EMBO J.* **25**, 3223–3233 (2006).
17. Håkansson, S., Galyov, E.E., Rosqvist, R. & Wolf-Watz, H. The *Yersinia* YpkA Ser/Thr kinase is translocated and subsequently targeted to the inner surface of the HeLa cell plasma membrane. *Mol. Microbiol.* **20**, 593–603 (1996).
18. Galyov, E.E., Håkansson, S., Forsberg, A. & Wolf-Watz, H. A secreted protein kinase of *Yersinia pseudotuberculosis* is an indispensable virulence determinant. *Nature* **361**, 730–732 (1993).
19. Juris, S.J., Rudolph, A.E., Huddler, D., Orth, K. & Dixon, J.E. A distinctive role for the *Yersinia* protein kinase: actin binding, kinase activation, and cytoskeleton disruption. *Proc. Natl. Acad. Sci. USA* **97**, 9431–9436 (2000).
20. Prehna, G., Ivanov, M.I., Bliska, J.B. & Stebbins, C.E. *Yersinia* virulence depends on mimicry of host Rho-family nucleotide dissociation inhibitors. *Cell* **126**, 869–880 (2006).
21. Dukuzumuremyi, J.M. *et al.* The *Yersinia* protein kinase A is a host factor inducible RhoA/Rac-binding virulence factor. *J. Biol. Chem.* **275**, 35281–35290 (2000).
22. Wiley, D.J. *et al.* The Ser/Thr kinase activity of the *Yersinia* protein kinase A (YpkA) is necessary for full virulence in the mouse, mollifying phagocytes, and disrupting the eukaryotic cytoskeleton. *Microb. Pathog.* **40**, 234–243 (2006).
23. Navarro, L. *et al.* Identification of a molecular target for the *Yersinia* protein kinase A. *Mol. Cell* **26**, 465–477 (2007).
24. Cooper, D.R. *et al.* Protein crystallization by surface entropy reduction: optimization of the SER strategy. *Acta Crystallogr. D Biol. Crystallogr.* **63**, 636–645 (2007).
25. Wang, H., Robinson, R.C. & Burtnick, L.D. The structure of native G-actin. *Cytoskeleton (Hoboken)* **67**, 456–465 (2010).
26. Fujii, T., Iwane, A.H., Yanagida, T. & Namba, K. Direct visualization of secondary structures of F-actin by electron cryomicroscopy. *Nature* **467**, 724–728 (2010).
27. Dominguez, R. Actin-binding proteins: a unifying hypothesis. *Trends Biochem. Sci.* **29**, 572–578 (2004).
28. Xue, B. & Robinson, R.C. Guardians of the actin monomer. *Eur. J. Cell Biol.* **92**, 316–332 (2013).
29. Ong, S.-E. & Mann, M. A practical recipe for stable isotope labeling by amino acids in cell culture (SILAC). *Nat. Protoc.* **1**, 2650–2660 (2006).
30. Ferron, F., Rebowski, G., Lee, S.H. & Dominguez, R. Structural basis for the recruitment of profilin-actin complexes during filament elongation by Ena/VASP. *EMBO J.* **26**, 4597–4606 (2007).
31. Burtnick, L.D., Urosev, D., Irobi, E., Narayan, K. & Robinson, R.C. Structure of the N-terminal half of gelsolin bound to actin: roles in severing, apoptosis and FAF. *EMBO J.* **23**, 2713–2722 (2004).
32. Chereau, D. *et al.* Actin-bound structures of Wiskott–Aldrich syndrome protein (WASP)-homology domain 2 and the implications for filament assembly. *Proc. Natl. Acad. Sci. USA* **102**, 16644–16649 (2005).
33. Lee, S.H. *et al.* Structural basis for the actin-binding function of missing-in-metastasis. *Structure* **15**, 145–155 (2007).
34. Bryan, J. Gelsolin has three actin-binding sites. *J. Cell Biol.* **106**, 1553–1562 (1988).
35. Gieselmann, R., Kwiatkowski, D.J., Janmey, P.A. & Witke, W. Distinct biochemical characteristics of the two human profilin isoforms. *Eur. J. Biochem.* **229**, 621–628 (1995).
36. Trülzsch, K., Sporleder, T., Igwe, E.I., Russmann, H. & Heesemann, J. Contribution of the major secreted yops of *Yersinia enterocolitica* O:8 to pathogenicity in the mouse infection model. *Infect. Immun.* **72**, 5227–5234 (2004).
37. Delorme-Walker, V. *et al.* Toxofilin upregulates the host cortical actin cytoskeleton dynamics, facilitating *Toxoplasma* invasion. *J. Cell Sci.* **125**, 4333–4342 (2012).
38. Aktories, K. Bacterial protein toxins that modify host regulatory GTPases. *Nat. Rev. Microbiol.* **9**, 487–498 (2011).
39. Calle, Y., Anton, I., Thrasher, A.J. & Jones, G.E. WASP and WIP regulate podosomes in migrating leukocytes. *J. Microsc.* **231**, 494–505 (2008).
40. Döppler, H. & Storz, P. Regulation of VASP by phosphorylation. *Cell Adh. Migr.* **7**, 482–486 (2013).
41. Nag, S., Larsson, M., Robinson, R.C. & Burtnick, L.D. Gelsolin: the tail of a molecular gymnast. *Cytoskeleton (Hoboken)* **70**, 360–384 (2013).
42. Li, D., Dammer, E.B., Lucki, N.C. & Sewer, M.B. cAMP-stimulated phosphorylation of diaphanous 1 regulates protein stability and interaction with binding partners in adrenocortical cells. *Mol. Biol. Cell* **24**, 848–857 (2013).
43. Groves, E. *et al.* Sequestering of Rac by the *Yersinia* effector YopO blocks Fc receptor-mediated phagocytosis. *J. Biol. Chem.* **285**, 4087–4098 (2010).
44. Park, S.K., Venable, J.D., Xu, T. & Yates, J.R. III. A quantitative analysis software tool for mass spectrometry–based proteomics. *Nat. Methods* **5**, 319–322 (2008).

ONLINE METHODS

DNA constructs. Inclusion of the membrane-localization domain (1–88) substantially increases insolubility[16]; thus, a YopO construct encompassing residues 89–729 was used in this study. *Y. enterocolitica* YopO and YopO mutants, and human VASP, EVL, gelsolin, CapG, Twf1, profilin and G1 were expressed in bacteria as N-terminal His_8-fusion proteins. YopO mutants were generated by QuikChange site-directed mutagenesis (Stratagene) according to the manufacturer's instructions. DNA encoding mDia1 (residues 583–1262) and WASP (150–502) were gifts from L. Blanchoin (iRTSV) and were expressed in bacteria with N-terminal glutathione S-transferase (GST) and C-terminal His_6 tags. Human Tmod3 was a gift from M. Hernandez-Valladares and was expressed in bacteria with N-terminal GST.

Protein purification. *Y. enterocolitica* YopO and YopO mutants and human proteins VASP, EVL, CapG, Twf1, profilin, gelsolin, gelsolin domain 1 and cofilin were purified to homogeneity by Ni-NTA affinity chromatography, cleaved with 3C protease and subjected to size-exclusion chromatography. Mouse diaphanous 1 (mDia1) (583–1262) and human WASP (150–502) were purified with sequential glutathione-Sepharose and Ni-NTA affinity chromatographies with their tags intact. Native Sf9 actin and cytoplasmic human actin were purified from Sf9 cells and HeLa S3 cells with GST-tagged gelsolin domains G4–G6, as previously described[45]. Rabbit skeletal-muscle actin was purified as previously described[25]. In the formation of the YopO–actin complex, Sf9 actin was mixed with YopO and purified by size-exclusion chromatography.

Protein crystallization. Cocrystals of YopO and rabbit muscle α-actin were attempted. However, unlike YopO–Sf9 cytoplasmic actin, YopO–rabbit α-actin does not form a stable complex on gel filtration, and correspondingly no crystal hits were obtained in crystallization trials. YopO WT (89–729)–Sf9 actin produced crystals readily under several conditions containing either PEG 8000, PEG 10000 or ethanol as precipitants, but crystals diffracted only to low resolution (~7 Å). Surface entropy–reduction mutations[46] targeting different regions of YopO were constructed with QuikChange site-directed mutagenesis (Stratagene). The mutant (K205Y E206Y E207Y K440Y K441Y) yielded crystals suitable for structure determination with the hanging-drop vapor-diffusion method with 200 nl of protein solution (10 mg/ml) in 200 nl of reservoir solution. The mutant crystallized in 0.1 M HEPES, pH 7.5, 30% PEG 400, and 0.2 M NaCl, and the crystals grew to maximal size over 10–14 d at 6 °C. One surface entropy–reduction mutation is involved in a crystal contact (**Supplementary Fig. 2a**). As such, it appears that the hydrogen bond involving Thr202 of Sf9 actin has an important role in the formation of a stable YopO–actin complex needed to form crystals, whereas the formation of ordered crystals with improved diffraction is dependent on the surface entropy–reduction mutations.

Structure determination. YopO–actin crystals were harvested by soaking in the mother liquor supplemented with 25% glycerol and then were flash frozen at 100 K. Crystals were screened at beamline I03 at the Diamond Light Source (DLS), and the final data were collected from improved crystals at beamline BL13B1 at the National Synchrotron Radiation Research Center, Taiwan (NSRRC) at a wavelength of 1 Å. Crystallographic data from the DLS were processed with xia2 (refs. 47,48) and scaled with AIMLESS[49], and data from the NSRRC were processed with HKL2000 (ref. 50) and scaled with SCALA[51]. The structure was solved by molecular replacement with Phaser as part of the PHENIX suite of crystallographic programs[52], with the atomic model of native actin (PDB 3HBT)[25] as a search model, then with the GDI domain (PDB 2H7O)[20], which had been subjected to normal mode analysis, and finally with the kinase domain (PDB 3KN6)[53] that had been trimmed by CHAINSAW[54]. Density modification was performed with Parrot[55]. Automated structure building and refinement were carried out with Phenix/Rosetta[56]. Manual building was performed with the graphics program COOT[57]. A composite omit map was generated to reduce model bias[58]. The MolProbity server (http://molprobity.biochem.duke.edu/) and validation tools present in COOT were used to assess the quality of the models at each stage of refinement. 97.8% of the residues in the final model were in the Ramachandran favored regions, 2.2% were in the additionally allowed regions, and there were no Ramachandran outliers.

Actin polymerization assay. Pyrene-actin polymerization assays were carried out with 2 μM Sf9 or rabbit skeletal-muscle G-actin (10% pyrene labeled). The reactions were assayed in 96-well, black, flat-bottomed plates (Corning, Nunc). Polymerization was induced with the addition of 10 μl of 10× KMEI polymerization buffer (500 mM KCl, 10 mM $MgCl_2$, 10 mM EGTA, and 100 mM imidazole-HCl, pH 7.0) in a total volume of 100 μl, and the fluorescence intensities were measured at wavelength 407 nm after excitation at 365 nm with a Safire2 fluorimeter (Tecan).

Pointed-end capping assays. Gelsolin–actin seeds were prepared by mixture of 10 μM Sf9 G-actin with 1 μM gelsolin in the presence of 1 mM $CaCl_2$. 4.5 μM Sf9 actin (10% pyrenyl labeled) was added to gelsolin–actin seeds (50 nM gelsolin and 0.5 μM actin) and polymerized in KMEI buffer for 2 h at room temperature. Various concentrations of human tropomodulin-3 and YopO were added, and depolymerization was initiated by dilution of the preassembled actin filaments by ten-fold in 2 mM HEPES, pH 7.6, 0.2 mM ATP, 0.5 mM DTT, 0.1 mM $CaCl_2$, 1 mM Na azide, 50 mM KCl, 1 mM $MgCl_2$, 1 mM EGTA, and 10 mM imidazole-HCl, pH 7.0, such that the final actin concentration was 0.5 μM in a total volume of 200 μl, and the fluorescence intensities were measured at a wavelength of 407 nm after excitation at 365 nm with a Safire2 fluorimeter (Tecan).

SILAC mass spectrometry. 'Heavy' and 'light' lysates were prepared from Raw264.7 cells grown respectively in either heavy isotopic [$^{13}C_6$]arginine and [$^{13}C_6$]lysine or normal isotopic [$^{12}C_6$]arginine and [$^{12}C_6$]lysine (Cambridge Isotopes). His_8-tagged YopO immobilized on Ni-NTA beads was used to pull down binding proteins from 'heavy' lysates, while in parallel an equivalent amount of empty beads were used against 'light' lysates for 3 h at 6 °C. After extensive washes, YopO was liberated from the beads via cleavage with 3C protease.

In-gel digestion and sample preparation for LC-MS/MS analysis. The following was carried out by the Sanford-Burnham Proteomics Facility. Samples were reduced and alkylated in a final concentration of 50 mM DTT and 50 mM iodoacetamide before digestion by trypsin. Trypsin was added to a final concentration of 25 ng/μl in 50 mM ammonium bicarbonate and left on ice for 1 h, then incubated for 16 h at 37 °C with shaking for complete digestion. The resultant tryptic peptides were extracted from SDS-PAGE gels according to the following elution process: 200 μl of water was added to the excised gels, which were sonicated for 10 min in a water bath and extracted once in 5% formic acid in water, four times with 50% acetonitrile in 5% formic acid in water, once in 70% acetonitrile and once in 100% acetonitrile. All extracted peptides were pooled together and vacuum dried and redissolved in 20 μl of 0.1% TFA. The tryptic peptides were then concentrated and desalted with a Millipore C18 Zip Tip (Millipore). The eluate was then vacuum dried and redissolved in 100 μl of LC/MS loading buffer (2% acetonitrile in 0.1% formic acid in water).

Protein identification and SILAC quantification analysis by 1D LC-MS/MS and IP2-Census. 20–25 μl of tryptic peptides were subjected to online LC-MS/MS, consisting of a Bruker-Michrom paradigm HPLC, a Zorbax C18 peptide-trap column (Agilent technologies), a 15-cm Michrom Magic C18 column, a low-flow ADVANCED Michrom MS source and a LTQ-Orbitrap XL (Thermo Fisher Scientific). A 90- and 120-min gradient of 10–27% B (0.1% formic acid and 100% acetonitrile) was used to separate the peptides; the total LC time was 110 and 140 min respectively. The LTQ-Orbitrap XL was set to scan precursors in the Orbitrap FTMS with a resolution of 60,000; this was followed by data-dependent MS/MS of the top four precursors. The LC-MS/MS raw data were analyzed by Integrated Proteomics Pipelines (IP2) version IP2 1.01 (Integrated Proteomics Applications, developed by J. Yates' team) with ProLucid algorithm as the search program for peptide/protein identification[59]. ProLucid search parameters set up to search the EBI.IPI.Mouse.v.3.84 fasta protein database include reversed protein sequences, with trypsin as the enzyme, with an allowance of up to two missed cleavages, semitryptic search and precursor mass tolerance of 50 p.p.m. The differential search included 57 Da for cysteines to account for carboxyamidomethylation in case of alkylation of cysteines in static mode; 16 Da for methionine oxidation, 79.9 Da for phosphorylation of serines, threonines and tyrosines; and lysine ubiquitination with a GG tag (114 Da); these modifications were identified with a maximum allowance of two post-translational

doi:10.1038/nsmb.2964

modifications per peptide. Metabolic-labeling search was enabled with R10 and K8. The search results were viewed, sorted, filtered, and statically analyzed with DTASelect with a Precursor delta mass cutoff of 50 p.p.m. (ref. 60) and false discovery rate (FDR) of less than 2.0%. Differential metabolic proteomics data analysis was carried out by IP2-Census[44].

Size-exclusion chromatography of ternary complexes. All size-exclusion chromatography runs were performed on a Superdex 200 HR 10/300 column (GE healthcare) in gel-filtration buffer containing 2 mM HEPES, pH 7.6, 100 mM NaCl, 0.2 mM ATP, 0.5 mM DTT, 0.1 mM $CaCl_2$, and 1 mM Na azide. Proteins YopO WT (150 μg); Sf9 actin (90 μg); profilin (64 μg); G1 (30 μg); cofilin (72 μg); CapG (66 μg) or protein mixtures YopO WT (150 μg) and Sf9 actin (90 μg); YopO WT (150 μg), Sf9 actin (90 μg) and G1 (60 μg); YopO WT (150 μg), Sf9 actin (90 μg) and profilin (96 μg); YopO WT (120 μg), Sf9 actin (72 μg) and cofilin (108 μg); and YopO WT (120 μg), Sf9 actin (72 μg) and CapG (132 μg) were adjusted to 110 μl in 2 mM HEPES, pH 7.6, 0.2 mM ATP, 0.5 mM DTT, 0.1 mM $CaCl_2$, and 1 mM Na azide. Protein mixtures were allowed to complex for 30 min on ice. Samples were centrifuged at 21,000*g* for 30 min, after which 100 μl was injected. Gel-filtration runs were performed at a flow rate of 0.5 ml/min at 15 °C. Selected fractions of the eluted material were analyzed on SDS-PAGE and visualized by Coomassie staining.

***In vitro* phosphorylation.** YopO or YopO mutants (4.7 μM), were mixed with G-actin (4.7 μM) in the presence or absence of substrates (4.7 μM) and/or G1 (14.1 μM) or profilin (14.1 μM), and adjusted to 10 μl in 2 mM HEPES, pH 7.6, 0.2 mM ATP, 0.5 mM DTT, 0.1 mM $CaCl_2$, and 1 mM Na azide. In the substrate-phosphorylation assays, all substrates tested were full-length proteins without fusion tags except for mDia1 (residues 583–1262) and WASP (150–502), which contained both an N-terminal GST and a C-terminal His_6 tag. The reaction was initiated by addition of an equal volume of kinase buffer containing 40 mM HEPES, pH 7.6, 2.0 mM ATP, 2 mM DTT, 20 mM $MgCl_2$, and 4 mM $MnCl_2$, supplemented with 5 μCi of [γ-^{32}P]ATP. The phosphorylation reactions were allowed to take place for 30 min at 30 °C and were terminated by the addition of SDS-PAGE sample buffer and heating for 5 min at 95 °C. For WASP in particular, because it migrated at a similar position on SDS-PAGE as YopO, thrombin protease was added postphosphorylation to remove the GST tag. Proteins were separated by SDS-PAGE and visualized by Coomassie staining, and radioactivity in the dried SDS-PAGE gels was visualized by exposure to X-ray film.

Phosphorylation of VASP for actin polymerization assay. VASP (2.5 μM) was preincubated with YopO or YopO KD (1.25 μM) in the presence of Sf9 actin (1.25 μM) at 30 min at 30 °C in 20 mM HEPES, pH 7.6, 1.0 mM ATP, 1 mM DTT, 10 mM $MgCl_2$, and 2 mM $MnCl_2$ to allow phosphorylation to take place. In parallel, for the –ATP control, VASP was mixed with YopO and Sf9 actin in the absence of ATP, $MgCl_2$ and $MnCl_2$, and was left on ice. The YopO-phosphorylated VASP or the controls were added to the pyrene-actin polymerization reaction containing rabbit muscle α-actin (2 μM, 10% pyrene labeled) and 2.8 μM profilin. VASP and YopO (or YopO KD) were present in the actin polymerization reaction at final concentrations of 0.25 μM and 0.125 μM, respectively.

45. Ohki, T., Ohno, C., Oyama, K., Mikhailenko, S.V. & Ishiwata, S. Purification of cytoplasmic actin by affinity chromatography using the C-terminal half of gelsolin. *Biochem. Biophys. Res. Commun.* **383**, 146–150 (2009).
46. Goldschmidt, L., Cooper, D.R., Derewenda, Z.S. & Eisenberg, D. Toward rational protein crystallization: a Web server for the design of crystallizable protein variants. *Protein Sci.* **16**, 1569–1576 (2007).
47. Kabsch, W. Automatic processing of rotation diffraction data from crystals of initially unknown symmetry and cell constants. *J. Appl. Crystallogr.* **26**, 795–800 (1993).
48. Winter, G., Lobley, C.M.C. & Prince, S.M. Decision making in xia2. *Acta Crystallogr. D Biol. Crystallogr.* **69**, 1260–1273 (2013).
49. Evans, P.R. & Murshudov, G.N. How good are my data and what is the resolution? *Acta Crystallogr. D Biol. Crystallogr.* **69**, 1204–1214 (2013).
50. Otwinowski, Z. & Minor, W. Processing of X-ray diffraction data collected in oscillation mode. *Methods Enzymol.* **276**, 307–326 (1997).
51. Evans, P. Scaling and assessment of data quality. *Acta Crystallogr. D Biol. Crystallogr.* **62**, 72–82 (2006).
52. Zwart, P.H., Afonine, P.V. & Grosse-Kunstleve, R.W. Automated structure solution with the PHENIX suite. *Methods Mol. Biol.* **426**, 419–435 (2008).
53. Malakhova, M. *et al.* The crystal structure of the active form of the C-terminal kinase domain of mitogen- and stress-activated protein kinase 1. *J. Mol. Biol.* **399**, 41–52 (2010).
54. Stein, N. CHAINSAW: a program for mutating pdb files used as templates in molecular replacement. *J. Appl. Crystallogr.* **41**, 641–643 (2008).
55. Cowtan, K. Recent developments in classical density modification. *Acta Crystallogr. D Biol. Crystallogr.* **66**, 470–478 (2010).
56. DiMaio, F. *et al.* Improved molecular replacement by density- and energy-guided protein structure optimization. *Nature* **473**, 540–543 (2011).
57. Emsley, P., Lohkamp, B., Scott, W.G. & Cowtan, K. Features and development of Coot. *Acta Crystallogr. D Biol. Crystallogr.* **66**, 486–501 (2010).
58. Terwilliger, T.C. *et al.* Iterative-build OMIT maps: map improvement by iterative model building and refinement without model bias. *Acta Crystallogr. D Biol. Crystallogr.* **64**, 515–524 (2008).
59. Xu, T. *et al.* ProLuCID, a fast and sensitive tandem mass spectra-based protein identification program. *Mol. Cell. Proteomics* **5**, S174 (2006).
60. Tabb, D.L., Mcdonald, W.H. & Yates, J.R. DTASelect and Contrast: tools for assembling and comparing protein identifications from shotgun proteomics. *J. Proteome Res.* **1**, 21–26 (2002).